JOURNAL OF MATERIALS SCIENCE 32 (1997) 3613–3620

Mo surface enrichment on a Fe–Cr alloy by electron beam irradiation

M. KEDDAM, F. NENCI*, F. PILLIER, S. TOSTO*, C. VIGNAUD
UPR15 du CNRS ''Physique des Liquides et Électrochimie'' Tour 22, 4 place Jussieu, 75252 Paris Cedex 05 - France and **ENEA, C.R.E. Casaccia, Via Anguillarese 301, 00060 Roma - Italy.*

Mo alloying has been carried out on a Fe–Cr alloy by electron beam irradiation. It is shown that a Mo surface enrichment can be obtained in the range 2–8 at %. Scanning and transmission electron microscopy, X ray microanalysis and electron energy loss spectroscopy have been used to investigate the microstructures obtained after irradiation. Mo–Cr carbide and intermetallic χ phase have been identified after alloying. The intermetallic phase is preferentially formed when the Mo content increases. It is concluded from electrochemical studies and potentiostatic attacks that the active and transpassive dissolution rates are closely related to the Cr content in the ferritic phase. This work must be also regarded as a first step towards the surface preparation of 316 S. S. by Mo incorporation to 304 S. S.

1. Introduction

The present paper concerns the electron beam alloying of Mo on a substrate of Fe–Cr alloy. It is known that the addition of Mo improves the resistance to pitting of the Fe–Cr alloys in aqueous environments containing Cl^- ions [1].

The electron beam is widely recognized as a powerful tool to carry out thermal surface modification [2], cladding and alloying of metallic substrates [3, 4] and to consolidate metal coatings by surface melting [5]. Rapid solidification processing has been also investigated by means of electron beam treatment [6]. Controlled surface microstructures and chemical compositions of several alloys of technological interest have been obtained by electron beam processing of metallic bilayers [7, 8]. In this kind of treatment, a sheet of overlayer material is clamped onto a substrate and then submitted to electron beam irradiation. The power and interaction time of the beam are optimized to melt the overlayer together with a controlled thickness of substrate. The chemical composition and microstructure of the alloyed zone is determined essentially by the dilution of the alloy elements of the overlayer in the molten pool and by the diffusion of elements between overlayer and substrate across the liquid–solid interface. The alloying process is possible because the overlayer sheet melts first and then wets the substrate, thus ensuring the necessary thermal contact at the interface of the bilayer [9]. As a consequence, particular attention must be payed to the surface compositions of substrate and overlayer, because both affect that of the alloyed zone. Indeed, it is known that the technological materials have often different surface and bulk chemical composition not only because of the presence of oxides but also as a result of thermodynamic equilibrium conditions or non-equilibrium phenomena [10]. Surface segregation is widely reported [11]; moreover, amongst the mechanisms contributing to a surface chemical composition anomalous with respect to the bulk composition include: (i) the depletion of some elements, for instance Cr [12], and (ii) the surface pollution: for instance, C enrichment at the surface of steel sheets can be typically caused by the decomposition of lubricants adsorbed during hot rolling [13]. The local composition changes in materials at the contact surface of the bilayer become particularly evident when the concerned elements have a strong tendency to form compounds or precipitates. These can be easily recognized in the microstructure with the usual metallographic procedures. This is the case in the electron beam alloying of Mo, owing to the tendency of this element to form a variety of carbides in the presence of C [14]. The present paper is aimed at investigating the microstructure of the Fe–Cr alloy after alloying treatment with particular regard to the effects of the surface composition of the substrate.

2. Experimental procedure

2.1. Material elaboration

The substrate, Fe–Cr in the form of sheets 5 mm thick, was provided by IRSID. Its chemical composition is given in Table I. Thin sheets of molybdenum from Goodfellow, (99.9% purity and 25–50 μm thick), were used.

The overlayer material is melted with a strong remixing of the substrate. A new chemical composition is obtained at the surface depending on the depth of the substrate actually melted and on the thickness of the Mo foil, mechanically clamped onto the surface to be treated. The electron beam was monitored by an

0022–2461

TABLE I Chemical analysis of the Fe–Cr substrate: (1) provided by IRSID; (2) control analysis of C and N

	C	N	Mn	Si	S	Pb	Ni	Cr	Mo	Cu	Ti	Nb	Co
1	0.0210	–	0.5747	0.3468	0.0225	0.0210	0.4079	17.417	0.0818	0.0661	0.3400	0.0100	0.0236
2	0.0515	0.0450											

TABLE II Electron beam processing parameters

	Average concentration	Electron beam energy kV	Mo foil thickness μm	Number of passes
Alloy-A	2 at %	50	25	2
Alloy-B	8 at %	40	50	1

Alcatel (CEA Licence) assembly whose maximum power is 10 kW. The variable beam parameters are tension, current, travel speed i.e. interaction time, and number of passes. Table II presents the irradiation conditions to obtain a low or a high surface Mo content in the alloy, (respectively materials A and B).

2.2. Structural study

The structure of the surface layer was analysed on the Fe–Cr alloy as-received i.e. without any heat treatment, after melting with low or high Mo content and, for comparison purposes, after melting but without any elemental addition.

The first characterization was performed by scanning electron microscopy (SEM) observations (LEICA-440) on cross-sections of the melted zone. The secondary electron signal is used as the probe after the sample is chemically etched in a Kalling bath and the backscattered electron signal after a careful 3 μm diamond paste polishing. These observations are completed by X-ray analysis which investigates a sample size of a minimum of a few μm^3. In most cases this poor spatial resolution was not sufficient and the experiments were completed by nanoanalysis on thin foils by transmission electron microscopy (TEM) (Jeol model 2000 FX) with a LINK EDX system and a Gatan PEELS (Parallel Electron Energy Loss Spectroscopy) analyser. The PEELS spectroscopy is very sensitive thus allowing the detection of low atomic number elements such as C or N which are present in some particular types of precipitates. Due to the presence of intermetallics in the explored structures the ion milling technique (Gatan-Duo mill) was mandatory for thin foil preparation.

2.3. Electrochemical study

Electrochemical investigations were performed in a 0.5 M H_2SO_4 solution at 25°C. Potentiostatic attacks, either in the active or transpassive range, followed by SEM observations, evidenced selective dissolution or preferential intergranular corrosion. Electrochemical measurements were carried out on rotating disc electrodes prepared from short rods, 5 mm in diameter, cut out normal to the surface in the central part of the melted zone. Linear sweep potentiodynamic current–voltage curves were recorded and the rate of iron dissolution as Fe^{2+} was monitored with a rotating ring disc arrangement.

3. Results

3.1. Structural study

3.1.1. Low molybdenum content alloy (A)

The microstructure and the α grain size of the low molybdenum content alloy (called A) is evidenced after microetching in a Kalling bath. Fig. 1, obtained with secondary electrons, shows an unknown phase at the border-lines of the grain boundaries. The chemical composition of this phase, across a width of a few microns, does not differ from that of the bulk when it is measured, with poor spatial resolution, techniques such as EDX on MEB. A careful search on the thin foils was necessary in order to resolve the true fine structure of such an intragranular micro-precipitation. Electron diffraction patterns revealed the existence of a lamellar structure with alternated α and γ needles. Fig. 2, obtained with a 200 kV TEM, shows this α–γ alternance. The chemical composition of the α matrix grains and of some needles are reported in Table III. It appears that the chromium content of the parent metal is conserved in the coarse grains of the superficial layers where the molybdenum content is close to 2 at %. On the contrary the ferritic and austenitic needles are very rich in molybdenum (23–31 at %) but poor in chromium (10–12 at %). One can expect different electrochemical behaviours on these different parts of the electrode.

Figs 3 and 4 show the presence of many precipitates located specifically at the phase boundaries. Fig. 5 is an example of an electron diffraction pattern of one of these precipitates; it corresponds to a F.C.C (1 1 1) plane. The structure of all the precipitates observed in this alloy has been associated with a F.C.C. lattice with a 1.06 nm lattice parameter which may be compared to the known structure of $M_{23}C_6$ type carbides. The electron energy loss spectrum, Fig. 6, presents a well-defined carbon-K edge and this spectroscopy confirms the presence of carbon in all the precipitates. A specimen holder cooled with liquid nitrogen has been used in order to hinder contamination and avoid any confusion between a compositional carbon element and a contaminating one.

The chemical composition of these carbides was evaluated by EDX and the results are reported in Table III. However it is worth noting that the detector, a silicon–lithium crystal with an ultrathin window, is sensitive to the presence of both compositional

and contaminating carbon at room temperature carbon and thus values calculated by the ZAF quantitative program must be considered as only qualitative. The most important evidence is the high chromium content and a molybdenum level higher than the matrix one. Three EDX spectra are presented in Fig. 7. They show the chromium content (a) in the matrix, (b) within a carbide precipitate and (c) nearby it. The quantitative treatment of these spectra allowed us to observe a Cr depleted zone (10 at % instead of 18 at % in the matrix) in the proximity of the carbide precipitates. Close to each Cr–Mo carbide, in fact, there is a gradient of chromium concentration. The effect of this concentration gradient on electrochemical properties will be discussed in a later section of this paper.

3.1.2. Fe–Cr alloy as-received

The microstructure of the substrate has been investigated before any heat treatment. Kalling microetching showed a normal grain structure without lamellar α–γ needles. The thin foil observations exhibited precipitates whose electron diffraction pattern differs from that of the carbides identified previously. The electron energy loss study confirmed the absence of C but evidenced the presence of the nitrogen-K edge as is shown in the spectrum presented in Fig. 8. All precipitates analysed in this as-received alloy are of nitride type.

3.1.3. Substrate melted without any addition

The same beam conditions as previously described were used to heat-treat the Fe–Cr alloy substrate. Kalling microetching shows the same type of microstructure as observed with a Mo sheet (see Fig. 1) with micro-intragranular precipitation of a γ phase at the

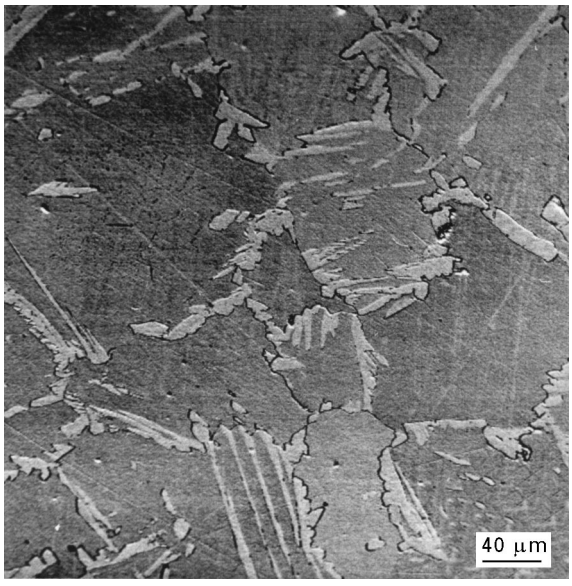

Figure 1 Kalling microetching observed by SEM – 2 at % Mo alloy.

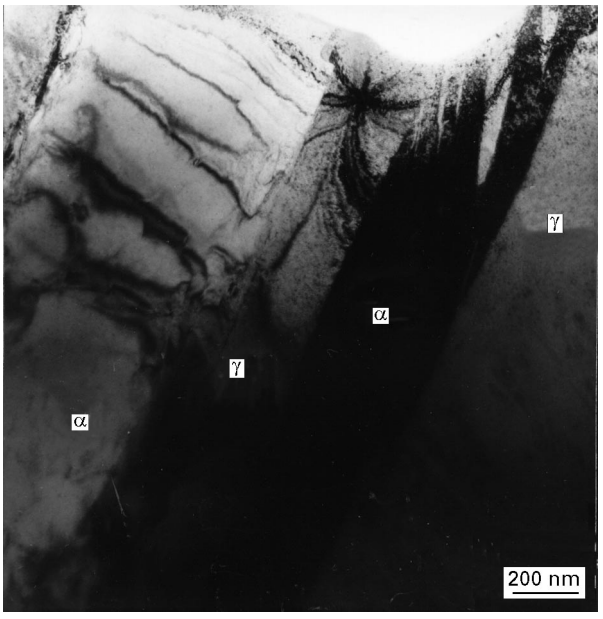

Figure 2 α–γ needles identified by TEM diffraction – 2 at % Mo alloy.

TABLE III EDX nanoanalysis on thin foils

	Mo		Cr		Fe		Si	
	at %	wt %	at %	wt %	at %	wt %	at %	wt %
2 at % Mo alloy.								
Bulk	1.7	2.9	18	17	80	80	0.1	0.5
Ferritic needles	31	42	12	10	55	47	2.3	1
Austenitic needles	23	35	14	11	60	52	3.2	1.5
8 at % Mo alloy								
Bulk	7	12	14	12	79	76	0.5	0.2
Intermetallic dendrites	20	30	18	14	62	55	0.9	0.4
Precipitates								
As received: Chromium nitride	0	0	90	90	10	10	0	0
Melted without Mo: Chromium carbide	0	0	60	60	40	40	0	0
2 at % Mo alloy: Chromium–molybdenum carbide	5	10	55	50	40	40	0	0

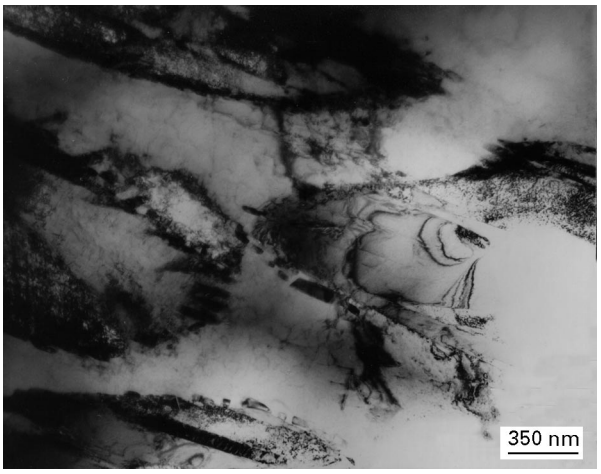

Figure 3 Interphase microprecipitates observed by TEM – 2 at % Mo alloy.

Figure 4 Chromium carbides observed by TEM – 2 at % Mo alloy.

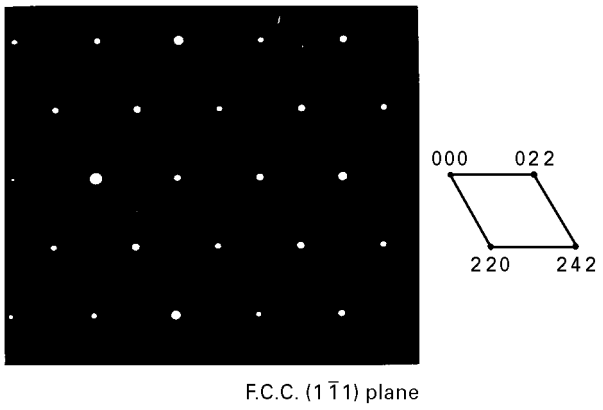

Figure 5 Electron diffraction pattern of an interphase precipitate – F.C.C. (111) plane – 2 at % Mo alloy.

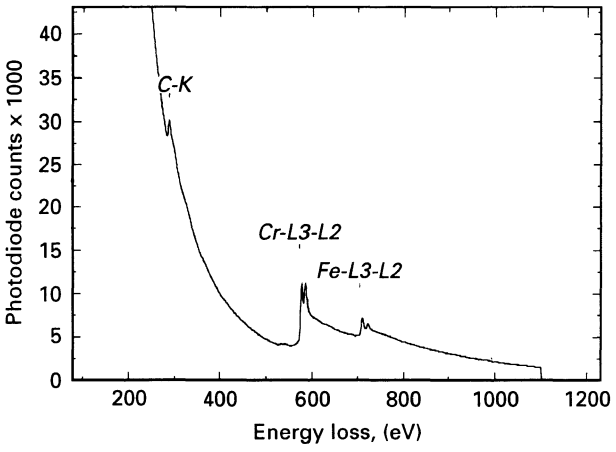

Figure 6 Electron energy loss spectrum of a precipitate – 2 at % Mo alloy.

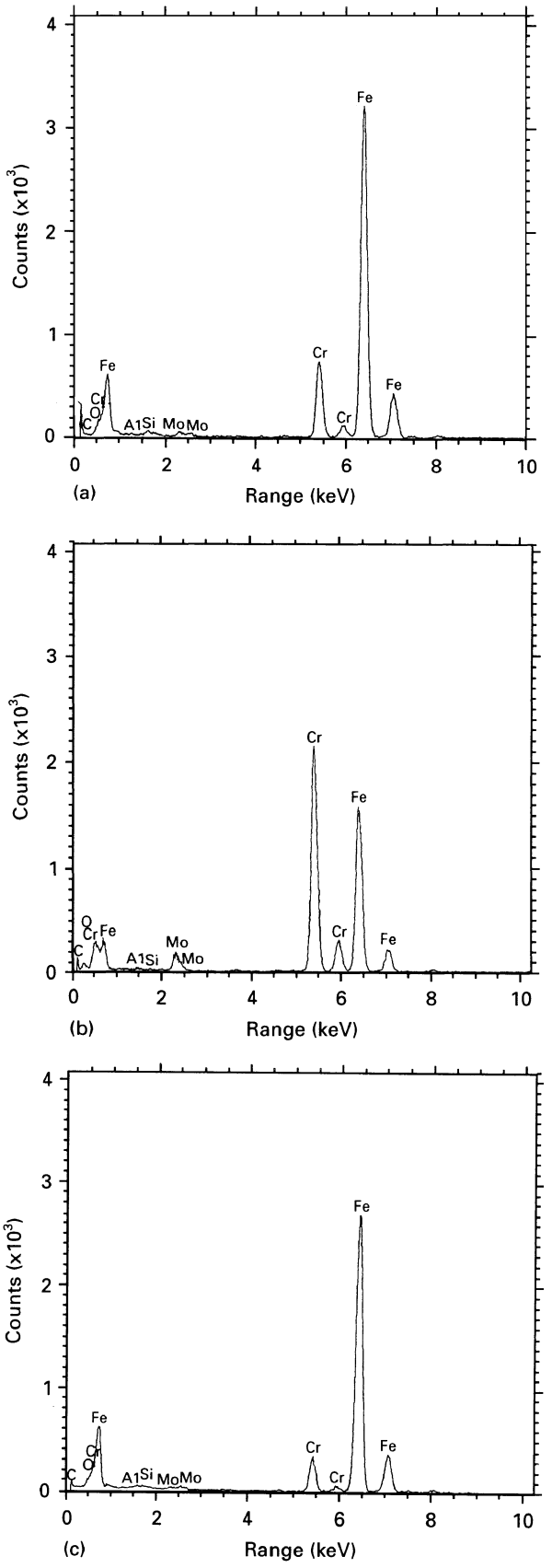

Figure 7 EDX spectra: (a) The bulk (18 at % Cr); (b) A precipitate (40 at % Cr); (c) Chromium depleted zone nearby this precipitate (10 at % Cr). 2 at % Mo alloy.

border-line of α boundaries. However all the precipitates analysed are carbides instead of nitrides in the as-received alloy.

This result allows us to conclude that this type of microstructure is induced by the beam melting and

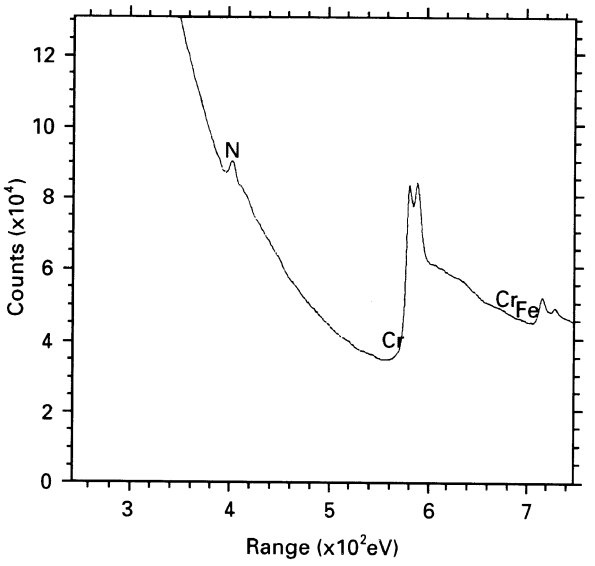

Figure 8 Electron energy loss spectrum of a precipitate – as-received alloy.

does not depend on any elemental addition. The quenching effects will be discussed in a later section of this paper. Molybdenum is not necessary but if added would favour this type of precipitation due to ultra rapid quenching.

The nominal carbon content of the substrate, 210 ppm, does not account for the presence of numerous carbide inclusions observed after electron-beam heat treatment. This is why we have carried out a new control analysis for C and N. These results are reported in the second line of Table I.

3.1.4. High molybdenum content (B)

The microstructure of the surface layers heat-treated with the beam conditions described above (Table I) was observed using SEM, with the backscattered electron detector. A phase, rich with a high atomic number element, presents a high white contrast as shown in Fig. 9 where a Mo rich dendritic structure is clearly identified.

The electron diffraction pattern shown in Fig. 10 was obtained on the crystal presented in Fig. 11. This diagram corresponds to a B.C.C. (1 1 3) plane. Several measurements on various crystals of this type allowed us to identify a B.C.C. structure with a 0.902 nm lattice parameter. The EDX nanoanalysis of these dendrites confirms the high molybdenum content. The results are reported in Table III. The mean Cr value is similar to the parent one, 18 at %, though the interdendritic zones are poorer in this element, 14 at %. The Mo content is 20 at % which is to be compared to the 7 at % Mo in the bulk. The dendritic structure can be compared to the χ phase structure described in the literature by Takeda and Yukawa [15] who studied the ternary system Cr–Fe–Mo and found for the chemical composition 50 wt % Fe, 20 wt % Cr, 30 wt % Mo a B.C.C. lattice parameter $a = 0.899$ nm. We have to note that such a dendritic structure has already been found in the case of Mo alloying on Fe–Cr–Ni alloy [16], with two types of Mo-rich intermetallic

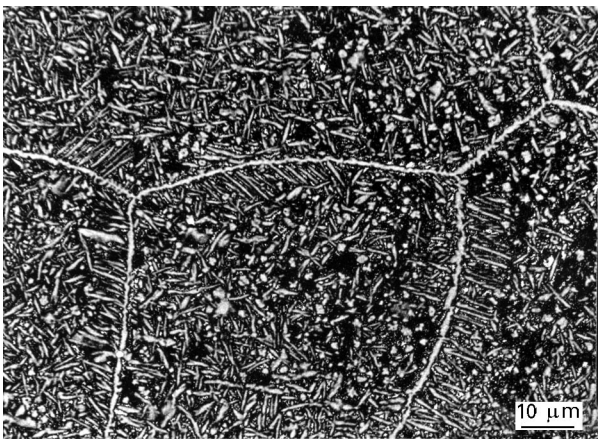

Figure 9 Microstructure observed by SEM backscattering – 8 at % Mo alloy.

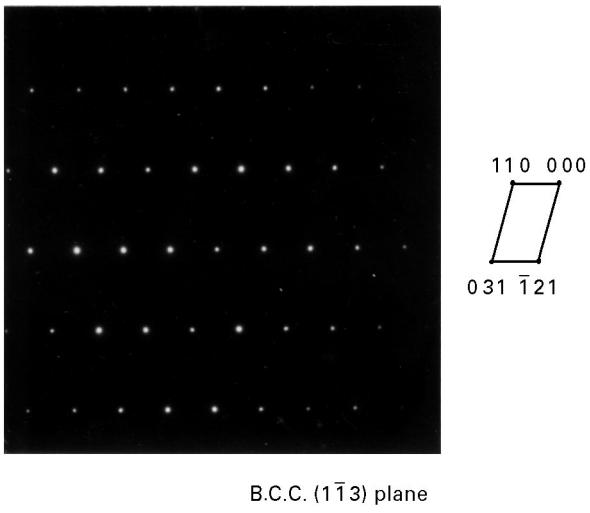

Figure 10 Electron diffraction pattern of a dendritic crystal – 8 at % Mo alloy – B.C.C. (113) plane.

Figure 11 Intermetallic crystal observed by TEM – 8 at % Mo thin foil.

dendrites being observed, one of them being similar to the χ phase. Though the Ni element is present in that case, no difference in the lattice parameter value was detected within the electron diffraction precision.

3.2. Electrochemical study

The potentiodynamic current–voltage curves recorded with a 33 mV s^{-1} sweeping rate are presented in Fig. 12. They deal with (a) the as-received Fe–Cr alloy (broken line); (b) the electron beam melted alloy without any addition (dash-dotted line); (c) the low molybdenum surface alloying (dotted line) and (d) the high molybdenum surface alloying (solid line).

We have to note the absence of an active peak in two cases: (a) as-received and (d) high molybdenum alloying. The presence of two peaks instead of one active peak in the two cases (b) and (c) is rather significant.

The transpassivity range begins at more anodic potentials in the three cases (b), (c), and (d) i.e. after beam processing under any conditions. The element Fe without chromium would present a high active peak together with a crystallographic attack though in the transpassive range the metal does not dissolve; only an oxygen evolution current may be observed. The chromium addition leads to a transpassive dissolution of the alloy. Chromium depleted areas described above may explain the presence of the two-peak active range registered in cases (b) and (c); such a feature is associated with chromium contents below 10 at % in the bulk Fe–Cr alloys [17].

3.2.1. Low molybdenum content alloy (A)

After a potentiostatic attack at a potential in the active range (− 850 mV/SSE) some of the needles exhibited a preferential dissolution as demonstrated in Fig. 13 obtained by SEM. It clearly shows α–γ needles with deep grooves corresponding to chromium depleted areas.

In the transpassive range, a potentiostatic attack reveals a general corrosion in all the α grains although the microprecipitates of α–γ phase are free of corrosion, as is shown in Fig. 14.

The result of RRDE (Rotating Ring Disc Electrode) experiments carried out on a 2 at % Mo alloy is shown in Fig. 15. The current–voltage curve of the disc electrode (material under investigation) displays a dissolution behaviour on the forward anodic scan successively in the active, passive and transpassive regions. The backward scan shows only a fully passive state of the alloy. The potential of the ring electrode was held at 0.8 V/SSE so that only divalent iron cations released by the disc dissolution are detected by their oxidation current to trivalent species. However

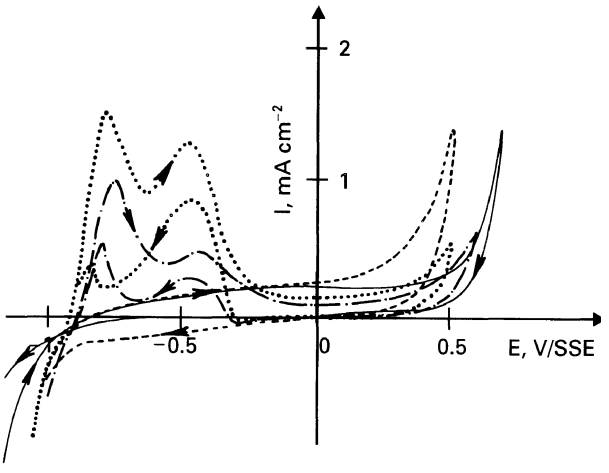

Figure 12 Current-voltage curves of Fe–Cr alloys: (-----), As-received alloy; (— · — ·) Melted without any addition; (·····) Low Mo surface alloying; (——) High Mo surface alloying. 0.5 M H_2SO_4.

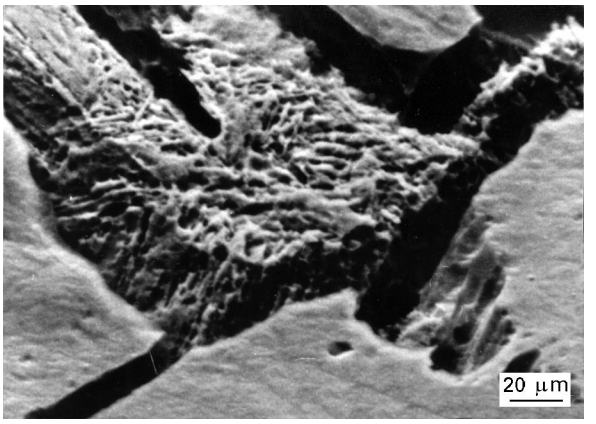

Figure 13 Potentiostatic attack, observed by SEM – 2 at % Mo alloy. (− 850 mV/SSE) 0.5 M H_2SO_4.

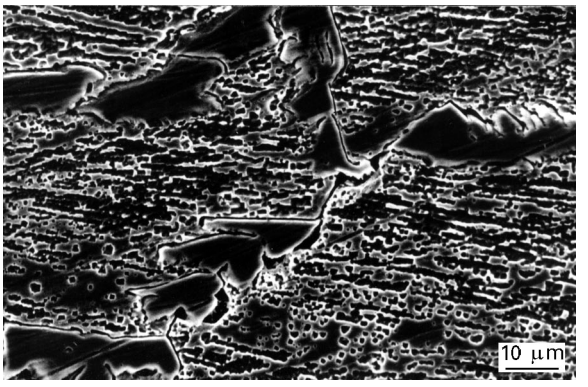

Figure 14 Potentiostatic attack, observed by SEM – 2 at % Mo alloy. Transpassivity – 0.5 M H_2SO_4.

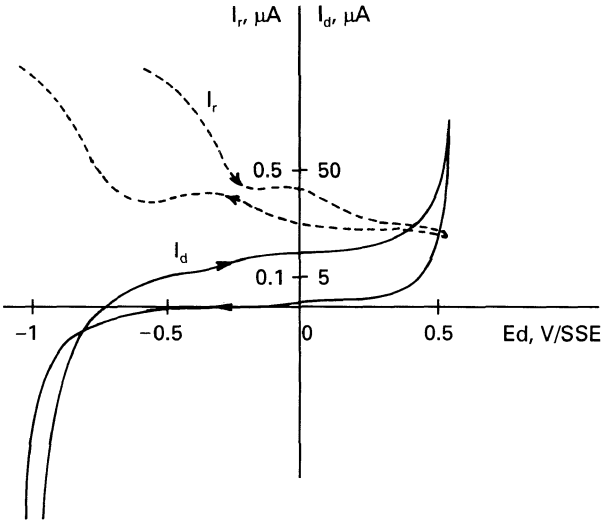

Figure 15 Current–voltage curve of the disc electrode (———), of the ring electrode (-----) 2 at % Mo alloy. 0.5 M H_2SO_4.

at the cathodic end of the potential domain the oxidation current at the ring electrode is due to the evolution of molecular hydrogen on the disc. On the forward scan the collection efficiency (ring current/disc current) is steadily decreasing from the active to the transpassive range. Taking into account the intrinsic collection efficiency of the device , 0.24, and the number of elementary charges exchanged at the disc and ring it can be concluded that at -0.5V/SSE the collection efficiency (0.095) of Fe^{2+} is in reasonable agreement with an homogeneous dissolution of the alloy. Dissolution in the passive domain gives rise to a slight maximum of the flux of Fe^{2+} associated to a much lower collection efficiency (0.025). Finally no increase at all of the ring current above the background is detected in the transpassive range in spite of a sharp rise of the alloy dissolution. An attempt to detect iron cations in the form of ferric species at a cathodic ring potential was totally unsuccessful. On the reverse scan a clear maximum of the Fe^{2+} flux is seen and is attributed to the reductive-dissolution of the passive film.

The potential dependence of the collection efficiency strongly supports the existence of various dissolution mechanisms depending upon the potential and the alloy composition. In the presence of low Mo content, active dissolution of the alloys takes place through a pure iron-like reaction path already established for Fe–Cr [18]. On the contrary, in the passive and even more clearly in the transpassive ranges the dissolution is entirely controlled by the presence of chromium. Iron oxidation products are not detected due to either selective dissolution of Cr or formation of highly stable Cr(VI)-bonded iron cations (poly chromates). These conclusions are in agreement with the relation put forward in the foregoing sections between phase composition and structural attacks at controlled potentials.

3.2.2. High molybdenum content alloy (B)

No corrosion can be detected in the active range as expected from the absence of an active peak. In transpassivity, we checked that the selective attack concerns the high molybdenum χ phase, present as dendrites or as a continuous path along grain boundaries (see Fig. 16).

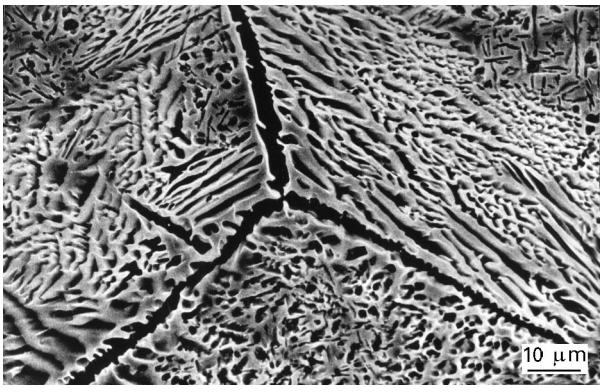

Figure 16 Potentiostatic attack, observed by SEM – 8 at % Mo alloy – Transpassivity – 0.5 M H_2SO_4.

4. Discussion

It can seem rather contradictory that in the transpassive range, Mo-rich dendrites are attacked though the Mo-rich α–γ needles do not corrode. In fact it is necessary to consider the Cr content of those different elements. The Mo-rich α–γ needles have a rather low chromium content (below 12 at %) though the dendritic intermetallic phase has a 18 at % Cr content like the parent alloy. It seems that chromium is the predominant element which governs the dissolution rate in activity and also in transpassivity: in the latter case chromium enhances the dissolution current though in the first case at a level larger than 12 wt % it inhibits the active current as seen previously.

In activity, the microprecipitates of α–γ phase are areas of lower corrosion resistance, due to a lower Cr content as described in [19]. This low Cr level can be explained by the numerous Cr carbides observed particularly in the α–γ phase boundaries. The carbon content of the bulk Fe–Cr, as verified by a second chemical analysis, is lower than 500 ppm and cannot explain such carbide precipitations. It was necessary to pay attention to the surface state of the different materials entering into the alloying process. SEM observations combined with X-ray analysis showed a C-rich surface layer which could be explained by the decomposition of lubricants deposited during Fe–Cr hot rolling.

5. Conclusion

The experimental results have shown that it is possible to obtain Mo enrichment at the surface of a Fe–Cr alloy by electron beam irradiation; the Mo content was found to range between 2–8 at %. Neither cracks nor pores have been observed in the alloyed zone within this range of composition. The anomalous C content at the surface of the Fe–Cr alloy (presumably due to cracking or decomposition of rolling oils during manufacturing) critically affects the microstructure after irradiation when the surface content of Mo is about 2 at %: carbide precipitation produces the Cr depletion seen in the alloyed samples. When the Mo concentration increases to average values of the order of 8 at %, the presence of zones with a local composition consistent with that of the intermetallic compound: 50 wt % Fe, 20 wt % Cr, 30 wt % Mo (χ phase) becomes more probable; this phase is preferentially formed with respect to the carbide. In this case, then, the role of carbon is less critical on the microstructure; in fact, under our experimental conditions, the formation of the intermetallic phase prevails over the formation of carbides even in the presence of an anomalous concentration of C at the surface of the substrate.

References

1. S. C. TJONG and J. B. MALHERBE, *App. Surf. Sci.* **44** (1990) 179.
2. S. SCHILLER and S. PANZER Annual Review of Materials Science, edited by R. A. Huggins, J. A. Giordmaine and J. B. Wachtman, (Annual Reviews Inc, Palo Alto, California, 1988) pp. 121–140.

3. R. ZENKER, "Surface Engineering with High Energy Beams", edited by A. P. Loureiro, O. Conde, L. Guera-Rosa and R. Vilar, (Trans. Tech. Publications, Brookfield, 1990) pp. 53–67.
4. D. G. RICKERBY, in ASM Heat Treatment and Surface Engineering Conference, 22–24 May, 1991 edited by E. J. Mittemeijer (Trans. Tech. Publications, Amsterdam, Zurich, 1992) p. 477.
5. T. R. TUCKER, J. D. AYERS and R. J. SCHAEFER, "Laser and Electron Beam Processing of Materials", edited by C. W. White and P. S. Bercy, (Academic Press, New York, 1980) pp. 760–767.
6. A. IWATA, A. TAUQIR and P. R. STRUTT, "Science and Technology of Rapidly Quenched Alloys", edited by M. Tenhover, W. L. Johnson and L. E. Tanner, Vol. 80, MRS Conference Publications (MRS, Pittsburgh, 1987) pp. 239–244.
7. S. TOSTO and F. NENCI, Mémoires et Études Scientifiques, Revue de Métallurgie, Juin 1987, pp. 311–320.
8. S. TOSTO, P. VANHILLE and C. VIGNAUD, *Surf. and Coatings Technol.* **58** (1993) 137.
9. S. TOSTO, F. NENCI and HU JIANDONG, in *J. Mater. Sci.* **29** (1994) 5852.
10. V. LAZARESCU, O. RADOVICI and M. VASS, *Appl Surf. Sci.* **55** (1992) 297.
11. T. S. SAMPATH KUMAR and M. S. HEGDE, *Appl. Surf. Sci.* **20** (1985) 290.
12. P. KOFSTAD, "High Temperature Corrosion", (Elsevier Applied Science Pub. Ltd, London 1988) p. 265.
13 S. TOSTO and S. GIRARDI, *Mat. Chem.* **7** (1982) 537.
14. T. B. MASSALSKI "Binary Alloy Phase Diagrams", (American Society for Metals, Metals Park, Ohio 1986) pp. 574–576
15. S. TAKEDA and N. YUKAWA, *J. Japan Inst. Metals*, **21** (1957) 275.
16. C. VIGNAUD, M. KEDDAM, F. PILLIER, S. TOSTO and F. NENCI, Materials Science Forum, Vol **126–128**. (1993) pp. 499–502.
17. I. EPELBOIN, M. KEDDAM, O. R. MATTOS and H. TAKENOUTI *Corros. Sci.* **19** (1979) 1105.
18. M. KEDDAM, O. R. MATTOS and H. TAKENOUTI, *Electrochim. Acta* **31** (1986) 1147, 1159.
19. P. LACOMBE, B. BAROUX and G. BERANGER, "Stainless Steels", (Editions de Physique, France, 1991) p. 26.

Received 6 February
and accepted 20 November 1995